In situ ultrasonic interface tracking for photovoltaic silicon directional solidification

Sophie Miralles, Mickael Albaric, Virginie Brizé, Philippe Guy, Bjarne Vincent, Jean-Paul Garandet, Daniel Henry, Valéry Botton

In situ ultrasonic interface tracking for photovoltaic silicon directional solidification

Sophie Miralles[a,*], Mickael Albaric[b], Virginie Brizé[b], Philippe Guy[c], Bjarne Vincent[a], Jean-Paul Garandet[b], Jean-Claude Willemetz[d], Daniel Henry[a], Valéry Botton[a]

[a] *Laboratoire de Mécanique des Fluides et d'Acoustique, CNRS/Université de Lyon, Ecole Centrale de Lyon/Université Lyon 1/INSA Lyon, ECL, 36 Avenue Guy de Collongue, 69134 Ecully Cedex, France*
[b] *Univ. Grenoble Alpes, CEA, LITEN, Campus Ines, 73375 Le Bourget du Lac, France*
[c] *LVA, INSA Lyon, 25bis Avenue Jean Capelle, 69621 Villeurbanne Cedex, France*
[d] *Signal Processing SA, Savigny, Switzerland*

Abstract

This paper presents an experimental validation of an *in situ* ultrasound technique for tracking the solid-liquid interface during directional solidification of photovoltaic silicon. Ultrasound bursts are introduced from the top into the melt via the tip of a carbon glass waveguide directly plunged into the liquid. Several runs of solidification have been conducted using the same waveguide thus demonstrating its reusability, its mechanical resilience and its appropriate acoustical and chemical compatibility with the melt. We present the times of flight analysis to track the location of the solid-liquid interface. As part of the signal crosses the solidifying ingot, we also measure c_s, the average celerity of sound waves in the solid. Since c_s exhibits a significant dependance on crystal orientation, we consider the possibility to use the echoes to extract some information on the crystalline orientation in the ingot. By quantifying the uncertainties and their dependence with the duration of the experiment in particular, we outline the conditions necessary to detect accurately the average orientation in the solid.

Keywords: A1. Directional solidification, A1. Characterization, A1. Interfaces, A1. Acoustic diagnostics, B2. Semi-conducting silicon

1. Introduction

Introducing MHz range ultrasounds in directional solidification processes may open numerous perspectives. The estimation of the position and velocity of the solid-liquid (s-l) front is a key issue for mastering solidification recipes, specially in the case of the photovoltaic industry, where the polycrystalline and mono-like silicon ingots have been increasing in size with years. Therefore the issue to monitor the (s-l) interface shape and position in time becomes more and more acute. However, for want of alternatives,

*Corresponding author
Email address: sophie.miralles@insa-lyon.fr (Sophie Miralles)

manual dipping of the interface using a silica-rod still appears to be the most used technique with the major drawbacks to be intrusive and to require experienced operators while not producing continuous inline data. A number of other methods to track the solid-liquid interface have been reviewed by Grujic *et al.* [1]; among these, the interface tracking using ultrasound pulses in a time of flight analysis is a promising technique, also in connection with industrial implementation. In this approach, ultrasounds are usually introduced in the process using a piezoelectric transducer which operates at ambient temperature far below the fusion temperature T_f of the grown material. A waveguide is then required to transfer the acoustic signal from the transducer to the material at T_f. Contactless solutions to create and detect ultrasounds have to be mentioned but are out of scope of this study, as these solutions require more complex and expensive setups featuring infrared lasers [2, 3], electromagnetic ultrasounds generators [4, 5] or direct visualisation in dedicated furnaces [6, 7, 8].

The solid material itself can be used as the waveguide. Indeed, both in the pioneering work of Parker and Maning [9] and in the works of Drevermann and co-workers [10, 11, 12], ultrasounds are introduced in the solid phase at the cold side of directional solidification furnaces. As a consequence, the sample cannot be fully melted since this would damage the ultrasound source. The authors consider different metallic alloys including doped silicon. Dold *et al.* [10] highlight the possibility of controlling the growth velocity by coupling the ultrasound measurements with the furnace control system. They monitor the (s-l) interface during the growth of doped silicon in a radiation-heated floating-zone furnace. A quartz glass rod is used for insulation between the transducer and the solid Si which has initially 300 mm length and 10 mm diameter. They also discuss in detail the variations of longitudinal and transverse sound velocities along this solid crystal with one end at less than 150 °C and the other end at more than 1400 °C.

Another option is to use a solid waveguide to introduce the ultrasounds from the hot side of the furnace directly into the melt. This method has demonstrated its interest in several configurations considering metallic alloys. In Al-based alloys, for example, ultrasounds are used for interface tracking [13, 14], but also particle detection [15], acoustic velocimetry [16, 17] and action on the process through acoustic streaming and cavitation [18, 19, 20]. A recurring issue is to define whether the waveguide has to be water-cooled. Another issue is to choose a material offering a satisfying compromise between chemical affinity with the melt, ensuring a good wetting, and high corrosion resistance but also keeping appropriate mechanical and acoustical properties over several hours and possibly several runs. Having an acoustic impedance similar to the melt impedance is also an advantage since this implies an optimum acoustic coupling. Trempa et al. [21] used a silica rod as a waveguide to drive ultrasounds into the liquid phase during Si solidification. Water is used both as a coolant of the ultrasonic transducer and as an acoustic coupling material between the transducer and the silica rod. Note that such a silica waveguide might lose its mechanical strength and react with the surrounding liquid Si, producing silicon oxide SiO. This could induce both the degradation of the waveguide and the contamination of liquid Si by oxygen, which could be detrimental to the grown silicon crystal quality.

Further uses of ultrasounds in melts can be considered in a long term perspective:

in situ diagnostics such as measurement and monitoring of the convective flow; *in situ* actions such as introducing stirring during solidification, often mentioned as acoustic streaming.

From this state of the art, our team has developed an ultrasonic waveguide solution to improve photovoltaic silicon elaboration processes [22, 23, 24, 25]. Essentially made of a carbon-glass rod, it does not require water cooling, has a good affinity with silicon and appropriate mechanical strength at temperatures higher than 1400 °C. The present paper describes a validation experiment for the suitability and the reusability of this device for tracking the interface of solidifying silicon. This (*s-l*) front tracking experiment has been performed in a small vertical Bridgman induction furnace, the BEATRICE furnace. It accepts typical Si loads of 100 g (see figure 1) and is operated at CEA INES in Chambéry, France. In the following section 2, the experimental apparatus and protocol are described. The section 3 is dedicated to the analysis of the echoes in a fully melted silicon. Section 4 presents the validation of our waveguide capabilities to track the (*s-l*) moving interface but also the opportunity it offers concerning inline, *in situ*, detection of crystalline orientation. Section 5 provides supplementary information concerning the crystal orientation effectively observed in this experiment.

2. Experimental apparatus and protocol

The waveguide has been designed and manufactured according to reference [26]. It is essentially a rod made of carbon glass V25 from Mersen™. This material (95 % of carbon) has undergone a thermal annealing at 2500 °C in order to keep stable thermomechanical properties at the operating temperatures of Si growth, which are slightly higher than 1414 °C. Its surface presents only very few open porosities. It also has a very good affinity with silicon: its wetting by liquid silicon results in the formation of a very thin layer of silicon carbide (SiC) on the imbedded surface [27, 28]. This SiC layer is itself wetted by the liquid silicon, which naturally ensures a good mechanical contact with the waveguide; this feature is illustrated on the photograph of figure 1 by the presence of a pending drop at the tip of the waveguide extracted from the melt few seconds earlier.

The velocity of longitudinal and transversal waves of carbon glass have been measured on a sample cylindrical rod of 8 mm in diameter and a length of 153.35 mm. We used contact transducers of 5 mm in diameter and a central frequency of 5 MHz for the longitudinal waves transducer and 2.25 MHz for the shear waves transducer. The transducers were excited by very short pulses. The electronic damping has been chosen to get very short echoes. The transducers were successively bonded to one side of the rod and used in a pulse-echo configuration. Then the velocity of ultrasonic waves was deduced from the measured time of flight between two successive reflexions from the opposite side of the rod. The values are 4337 $m.s^{-1}$ for longitudinal wave and 2645 $m.s^{-1}$ for the transversal waves. The error on these velocity measurements can be evaluated to less than 1 %. The mass density of the material is 1500 $kg.m^{-3}$.

For the waveguide used in the furnace, a piezoelectric pad (provided by Signal Processing SA) is glued directly at one end of the carbon glass rod of 10 mm in diameter and approximate length 500 mm, to emit and receive the 4.5 MHz burst signal.

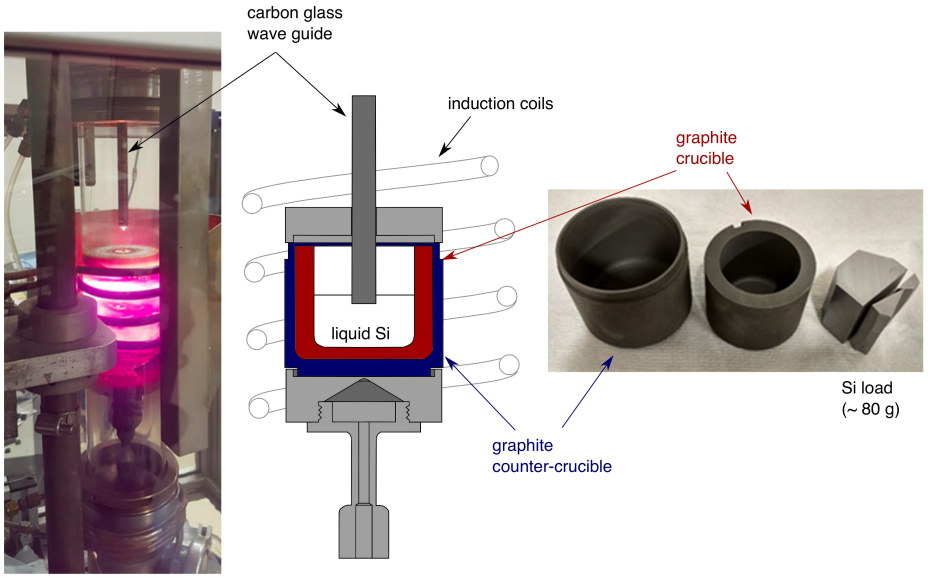

Figure 1: Left: photograph of the apparatus: the induction furnace contains a melted silicon load; a silicon drop still hangs at the tip of the waveguide that has been dipped into the melt during several dozens of minutes before being removed. Middle: scaled illustration of the furnace in which the waveguide (dark grey rectangle), the graphite crucible (red) and the counter-crucible (blue) are represented. Right: the silicon load, the graphite crucible and the counter-crucible.

Let us recall that the acoustic intensity transmission coefficient for normal wave incidence between two semi-infinite media of respective acoustic impedance $Z_1 = \rho_1 c_1$ and $Z_2 = \rho_2 c_2$, is:

$$T_{\infty,\infty} = \frac{4 Z_1 Z_2}{(Z_1 + Z_2)^2} \tag{1}$$

As can be seen from the material properties in table 1, the transmission coefficient between carbon glass and liquid silicon near the fusion point is thus expected to be 96 % (considering the SiC layer to be too thin to have an influence).

The waveguide is inserted vertically from the top through the only access into the furnace. A graphite cylindrical crucible of inner diameter 40 mm and height 45 mm is used; the side wall is 15 mm thick while the bottom wall is 5 mm thick. Its weight is 96.6 g. It is set within a counter crucible, made of the same material, of inner diameter 55 mm, height 53 mm and weight 70 g. External walls are 8 mm thick. The 80.2 g silicon load originated from a mono-crystal grown in a CZ furnace.

The data acquisition chain simply consists in a wave generator emitting a burst every minute. The same transducer, mounted on the waveguide, is used to emit the bursts and listen to the echoes between two bursts. A digital scope HD06054-MS triggered by the wave generator records each burst and its echoes after travelling through the setup. We initially intended to use bursts constituted by three periods of a 4.5 MHz sine with

Material	c ($m.s^{-1}$) (longitudinal waves)	ρ ($kg.m^{-3}$)	$Z = \rho c$ (10^6 $kg.m^{-2}.s^{-1}$)	$T_{\infty,\infty}$
Carbon glass	4337	1500	6.51	
Liquid Silicon	3920	2570	10.07	0.96
Solid silicon (at melting temperature)	[7630 - 8600]	2310	[17.62-19.86]	[0.93-0.90]
Graphite crucible	3100	1770	5.49	[0.72-0.68]

Table 1: Sound wave celerity, density and acoustic impedance of the different materials in the set-up (from ref. ([9, 10, 29, 30, 31, 32, 33, 34]) and the resulting intensity transmission coefficients through the interfaces with normal incidence as if they were between infinite domains (see eq. (1)). The materials are sorted in the order of the path followed by the acoustic signal in the set-up. The range given for solid silicon celerity refers to crystal orientation (1 0 0) and (1 1 1) respectively ([9]) and are considered as upper and lower bounds. Consequently, acoustic impedance and transmission coefficient depending on the solid Si celerity are given as ranges. Celerity data for carbon glass have been measured experimentally and data for graphite have been extracted from times of flight.

10 V peak-to-peak amplitude. However due to the acoustic backing material made in epoxy, the emitted burst is significantly deformed and gives rise to a travelling double wave packet.
The same waveguide has been used for several preliminary experimental runs aiming at choosing the best emission and acquisition parameters for the validation run. This waveguide has thus worked in operating conditions during several hours in total while the tip was immersed in liquid Si slightly above the fusion temperature, T_f. The integrity of the waveguide has been visually examined and confirms the robustness and suitability of the material for this working fluid. Reusability remains the advantage of this new waveguide with its acoustic impedance matching with liquid silicon.

3. Echo analysis for fully molten silicon

In a preliminary experiment, involving a slightly larger Si load, the waveguide has been vertically displaced within a crucible full of liquid silicon with the objective to detect the echo at the interface between the liquid and the crucible. The received signal from the emitted burst is interpreted in terms of times of flight to detect the distance between the tip of the waveguide and the crucible. Thanks to the value of the acoustic reflection coefficient between liquid and graphite $r_{lg} = \frac{Z_l - Z_g}{Z_l + Z_g} = 0.29$, the interface echo, denoted I_1 has sufficient amplitude to be observed.

As an illustration, the received waveform when the tip of the waveguide is located at $e_{l_0} = 21$ mm from the crucible is depicted in top figure 2. First, two peaks labelled WG_1 and WG_2, corresponding to back reflections from the tip of the waveguide, are observed. They are expected to have constant times of flight for any position of the

waveguide. They are followed by noisy wave packets of smaller amplitude, labelled WG_3 and WG_4 which are attributed to multiple reflections of emitted signal. Around time of flight $t_f = 233$ μs, the peak labelled I_1 matches with a signal travelling into the liquid Si between the tip of the waveguide and the crucible surface. When the solid Si will grow (see section 4), this wave paquet will correspond to the solid-liquid interface and its time of flight will evolve with the growth of the solid Si layer. It is interesting to note that after $t_f = 235$ μs, a pair of echoes labelled C_1 and C_2 is received. Their times of flight are larger than the one associated with I_1; these echoes thus come from a wave which has crossed the crucible surface and travelled within the graphite bottom wall, consistently with the value of r_{lg}. After $t_f = 240$ μs, the signal becomes noisy because of acoustic waves interfering with each other.

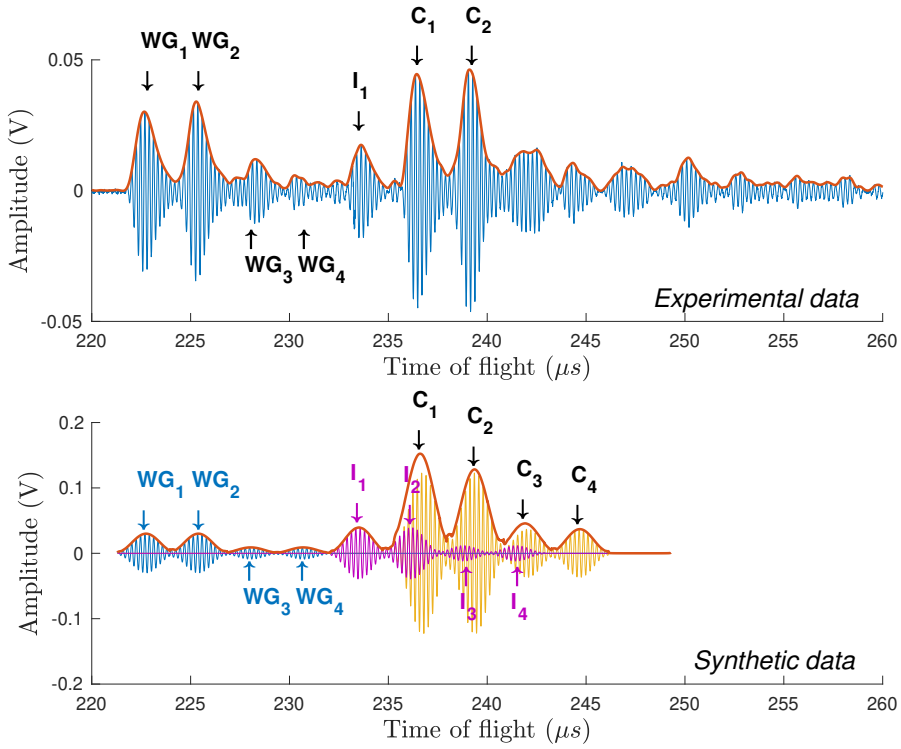

Figure 2: Top: experimental time series of the received signal when the silicon is fully liquid and the distance between the tip of the waveguide and the crucible is set to $e_{l_0} = 21$ mm. Echoes WG_1 to WG_4 are back reflections inside the waveguide. The echo I_1 is interpreted as the reflection at the crucible surface. Echoes labelled C_1 and C_2 corresponds to the reflections on the bottom of the crucible after crossing the 5 mm of graphite thickness. Bottom: synthetic data with calculated times of flight highlighting that echo I_2 is hidden by the echo C_1 in the experimental data (see text for details). Red curves are the envelopes of the signals.

A comparison with synthetic data built with Hamming window of 4.5 MHz sinusoidal signal is proposed in bottom figure 2. Arrival times have been calculated using

the thickness values and the material properties listed in table 1. One identifies the echoes WG_1 to WG_4 in blue, synthesized with 13 periods sine wave in hamming window with a 2.65 μs delay between each waveform. Amplitudes have been set to match the experimental signal. It is followed by two pairs of echoes I_1, I_2 and I_3, I_4 in purple starting from $t_{fI1} = t_{fWG1} + 2e_{l_0}/c_l \simeq 233.5$ μs considering waves travelling through the liquid Si layer of thickness $e_{l_0} = 21$ mm and with c_l the celerity of sound waves in the liquid Si. Times of flight of C_1 and corresponding delayed echoes are calculated by adding the travel across the bottom of the graphite crucible of thickness $e_g = 5$ mm: $t_{fC1} = t_{fI1} + 2e_g/c_g$ with c_g the celerity of sound waves in the graphite. The excellent matching of the synthetic data with the experimental ones in terms of times of flight, indicates that C_1 and C_2 can indeed be interpreted as waves crossing the bottom surface of the crucible before being reflected back. Note that, according to the synthetic data, the time of flight of I_2 is close to that of C_1, explaining why I_2 is not directly visible on the experimental signal. Actually, C_1 echo is a mix of the reflected wave at the bottom of the graphite crucible and the second echo I_2. As a first approach, the amplitudes of the synthetic signal have been estimated using the transmission/reflection coefficients with normal incidence for a single plane wave (see table 1). This framework makes the comparison between experimental and synthetic amplitudes less satisfactory than in terms of times of flight. Indeed, the WG_i amplitudes clearly appear to be too small in proportion with I_i and C_i. This could be attributed to a still better transmission coefficient from the waveguide to liquid silicon, which is already of 96% or even to the actual structure of the beam which is likely an angular distribution of plane waves, instead of a single plane wave. Note that total reflection is assumed at the bottom of the crucible so that energy is conserved, whereas further transmissions and reflections may occur in reality, leading to the experimentally observed complex signal after a time of flight of 247 μs.

The envelope of the signal is plotted as a full red line. It has been extracted from the time-series, using the *envelope* built-in function of Matlab™ and low-pass filtering the result with a 4 MHz cut off frequency. While the waveguide is moved vertically, the echo I_1 (with a time of flight denoted t_f) is tracked by applying a correlation algorithm between time series for each given position and a reference signal. The latter is taken when the waveguide tip was into contact with the crucible for which the time of flight for I_1 is denoted $t_{f,0}$. The delay $\tau = t_f - t_{f,0}$ corresponding to the maximum of the cross-correlation function was considered as the time of flight in the liquid between the waveguide tip and the crucible bottom. The celerity of ultrasounds in liquid silicon was taken as $c_l = 3920$ m.s^{-1} (see table 1). A measurement point was taken every 5 mm $\pm$ 1 mm from the bottom of the crucible to a maximum distance of 30.5 mm.

The result plotted in figure 3 depicts the reconstructed distance d from the time of flight as $2d = c_l\tau$ as a function of the distance mechanically measured. The agreement is excellent. The same cross-correlation technique will be used to extract the signal interface in silicon solidification run.
With this preliminary experiment, the waveguide is shown to be capable of emitting and receiving ultrasound bursts within the liquid silicon.

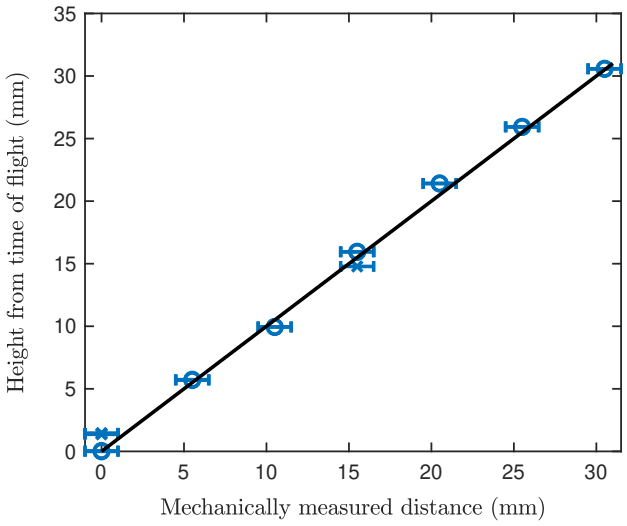

Figure 3: Preliminary echography in a graphite crucible containing liquid silicon. The waveguide tip is immersed in the melt and the time of flight associated to echo I_1 is measured using a cross-correlation approach to recover the distance between the waveguide and the crucible. The distances recovered from time of flight measurements are represented by blue circles 'o' when the waveguide is moved away from the crucible and by blue crosses '×' when it is displaced in the opposite direction. Horizontal error bars of 1 mm comes from the distance evaluated mechanically. The black line ($y = x$) corresponds to the expected prediction.

4. Solidification interface tracking

4.1. Front velocity estimation v_i

The next validation experiment is the tracking of the interface position during silicon growth. The waveguide tip was immersed in the melt and set at approximately 21 mm above the bottom. The induction heating power is decreased with a 50 °C/h ramp for 1 hour and then a 35 °C/h ramp during the measurements. The time $t = 0$ coincides with the beginning of the second cooling ramp. The first layer of solid silicon appears at $t_0 = 49$ min, according to the acoustic diagnostic.

The signal evolution during the solidification experiment is plotted in figure 4 as a spatiotemporal-like diagram. The colored level corresponds to the amplitude of the envelope of the received signal. The abscissa, graduated in microseconds, gives the time elapsed since the emission of a burst by the transducer, also referred to as the time of flight; the corresponding sampling rate is 100 MHz. The ordinate, graduated in minutes, gives the time elapsed since the beginning of the second cooling ramp; with a sampling rate of one minute. Note that a movie showing the signal evolution during the solidification experiment is attached to the online version of the present article as a supplementary material. As sound undergoes several echoes in the system, the received signal is complex, as described in the previous section. Before $t_0 = 49$ min, the crucible is full of liquid and the echoes emphasized in figure 2 are recovered. WG_1 and WG_2 are clearly visible at $t_f = 222.5\mu$s and $t_f = 225\mu$s. As the waveguide geometry is fixed all along

the experiment, these events correspond to constant time of flights and result in straight vertical stripes on the spatiotemporal diagram of figure 4.

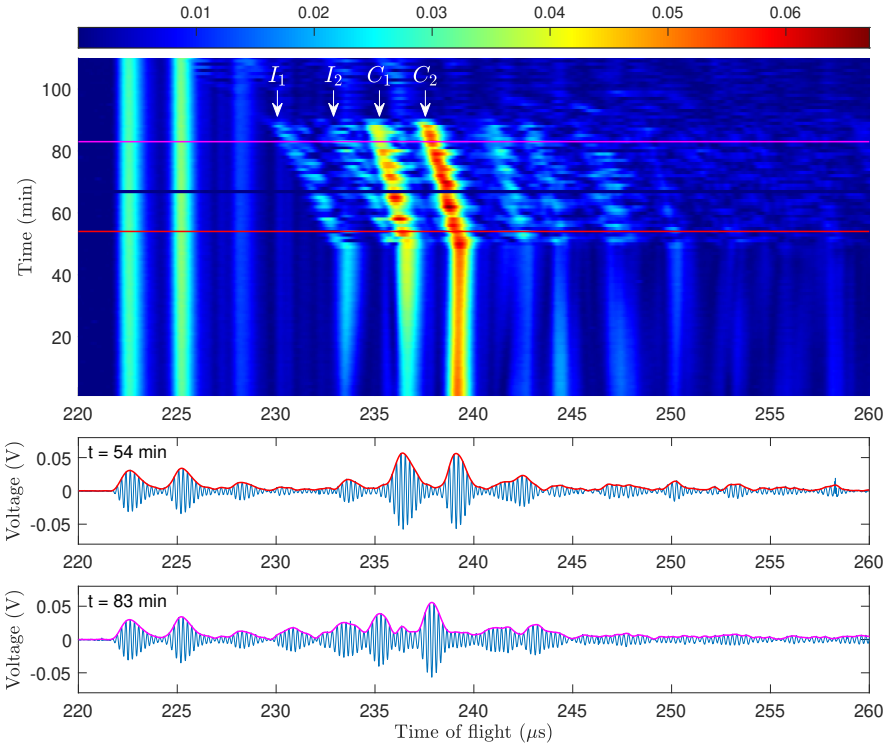

Figure 4: Top: Signal amplitude evolution during the solidification experiment. The color levels correspond to the magnitude of the received signal envelope (in red in fig 2). The horizontal axis indicates the time elapsed since the emission of a burst by the transducer, also referred to as the time of flight. The vertical axis corresponds to the time elapsed since the beginning of the recording. The echoes of interest have been labelled I_1, I_2, C_1 and C_2 and correspond to reflections on silicon (s-l) interface and crucible bottom surface respectively. Middle: Time series of the received signal at $t = 54$ min, few minutes after the start of solidification. Bottom: Times series for $t = 83$ min (corresponding to the purple horizontal line in the top diagram).

The event labelled I_1 in figure 2 is attributed to the acoustic reflection occuring at the (s-l) interface. After roughly 50 minutes of acquisition, the solidification is observed to start. As it can be seen in figure 4, this I_1 event shifts leftward as the solidification progresses, which corresponds to the upward motion of the solid-liquid silicon interface. As the solid layer grows, the signal reflected at the interface undergoes a smaller distance therefore yielding a smaller time of flight. The echo I_2, hidden by C_1 before the solidification begins, becomes clearly dissociated from C_1 after $t_0 = 49$ min; with the same slope as I_1. The two most significant events labelled C_1 and C_2 are attributed to

the reflections at the graphite crucible bottom surface after being transmitted through the solid Si layer and graphite crucible bottom thickness. Indeed, C_1 and C_2 shift leftward with a less important slope than the (s-l) interface (echo I_1 and I_2). This is due to the significant difference in sound wave celerity between the solid and the liquid silicon: a straightforward time of flight calculation shows that the theoretical slope ratio is $\frac{(c_s - c_l)}{c_s}$, where c_s denotes the celerity of sound in the solid silicon layer. Interestingly, information concerning the celerity of sound in the grown crystal is therefore contained in the time of flight of C_1 and C_2 echoes (see further developments in section 4.2).

We can see that the amplitudes of I_1 and I_2 are smaller than the amplitudes of C_1 and C_2; this is consistent with the small value of the estimated energy reflection coefficients $(1 - T_{\infty,\infty})$ at the interface between liquid and solid silicon (or even solid graphite). As observed in figure (4), a significant loss of signal occurs after 90 minutes of experiment. The reasons for this loss of signal are unclear: a significant curvature of the interface due to solidification from both bottom and side of the crucible, but more likely a solid silicon chunk has grown at the tip of the waveguide, deteriorating the acoustic signal.
Interestingly, successive minima and maxima are observed on the I_1, I_2, C_1 and C_2 echoes as the solidification evolves. They appear as nearly periodic patterns and might be attributed to finite thickness layer effects: maxima are indeed expected when the solid silicon thickness corresponds to multiples of the half acoustic wavelength in the solid ($\lambda = c_s/f_0 \simeq 1.9$ mm). As the solid silicon grows from zero to 25 millimeters on the whole experimental observation, the final thickness of the solid silicon layer is indeed not far greater than the acoustic wavelength ($\sim 26\lambda/2$), possibly explaining the occurrence of the amplitude variations.

The local maxima of the echoes corresponding to I_1, I_2 have been detected and followed during 42 minutes after the beginning of solidification. The resulting data have been converted into solid Si layer thickness, $e_{Si} = \frac{c_l \tau}{2}$ with $\tau = t_{f,I_i}(t_0) - t_{f,I_i}(t)$ the difference of time of flights between a given time t and the reference time t_0 associated with the beginning of solidification. The results are plotted in figure 5(a). The blue and red '$\times$' symbols correspond to data from I_1 and I_2, respectively, assuming $c_l = 3920$ m.s^{-1}. The evolution of the solid thickness is modeled as a linear function within the observed time, giving a constant average interface velocity $v_i = 9.23$ mm.h^{-1}, a value in excellent agreement with manual dipping performed in previous crystallization runs, with the same thermal recipe. Dispersion of maximum values of echoes can be due to small departure from planar interface.

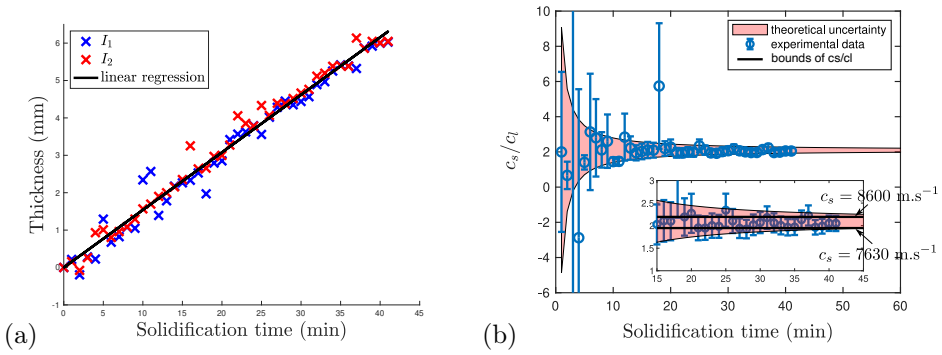

Figure 5: (a) Solid Si layer thickness evolution during the solidification experiment. '×' symbols correspond to echoes from the (s-l) interface assuming $c_l = 3920$ m.s^{-1}. Colors correspond to the analysis of first and second wave packets I_1 and I_2. The linear regression in solid black line gives the front velocity $v_i = 9.23$ mm.h^{-1}. (b) Ratio of sound celerities in the solid and liquid silicon as a function of time obtained by analyzing the times of flight of the echoes I_1 and C_1 (see eq.(2)). The error bars correspond to a standard error propagation formula considering a constant overestimated discrepancy on the time of flight detection, $\Delta\tau = 0.1\mu$s. The red shaded area is the confidence interval estimated from eq.(3) (assuming a constant interface velocity) and arbitrarily centered on the value deduced from $c_s = 8200$ m.s^{-1}. The inset is a zoom over the last 30 minutes of solidification. The solid black lines are the upper and lower bounds of c_s/c_l for the (1 1 1) and (1 0 0) grain orientation estimated from literature, meaning $c_s = 7630$ and 8600 m.s^{-1}, respectively, and with $c_l = 3920$ m.s^{-1}.

4.2. Crystal properties from acoustical measurements

The peculiar acoustic boundary conditions in our experiment allows the ultrasound bursts to be well transmitted through the grown crystal and the graphite crucible before being efficiently reflected, giving the strong echoes C_1 and C_2. The analysis of times of flight associated to these echoes can give valuable information on the properties of the grown solid, especially the sound wave celerity c_s. As already mentioned in table 1, the celerity of longitudinal waves for solid silicon depends on the crystal orientation and takes values between 7630 m.s^{-1} for (1 0 0) orientation, 8370 m.s^{-1} for (1 1 0) orientation and 8600 m.s^{-1} for (1 1 1) orientation. The relative difference between the bounds of c_s is thus only of about 12%. Extracting a valuable information on the crystalline orientation in the ingot from the acoustic signal thus requires a very accurate measurement of c_s. In the following, the uncertainties on the sound celerity in the solid ingot are reported. We will consider only the first echo from the double wave packet, but the reasoning remains the same for the second one. For a given time t, the thickness of the solid layer can be expressed with both the time of flight τ associated to I_1 and the time of flight τ associated to C_1: $e_{Si}(t) = \frac{c_l}{2}\tau_I(t) = \frac{c_l c_s}{2(c_s - c_l)}\tau_C(t)$. From these equations, we can express the ratio of the sound celerities in the solid and liquid silicon as:

$$\frac{c_s}{c_l} = \frac{\tau_I}{\tau_I - \tau_C} \tag{2}$$

This quantity is displayed as a function of time in figure 5(b). The blue circles representing the experimental data show a large scatter during the first minutes of solidification when the thickness of the crystal does not exceed 1.5 mm. The uncertainties on this quantity are related to the uncertainty in the detection of times of flight. As the maximum amplitude of the wave packets on the acoustic signal is not very peaked, the uncertainty of the correlation algorithm is estimated to be around half a period of the acoustic signal ($\Delta\tau = 1/(2f) \simeq 0.1\mu$s). The relative uncertainty plotted as error bars in figure 5(b) is given by:

$$\frac{\Delta(c_s/c_l)}{c_s/c_l} = \frac{\Delta\tau_I}{\tau_I} + \frac{\Delta\tau_I + \Delta\tau_C}{\tau_I - \tau_C} \tag{3}$$

Assuming $\Delta\tau_I = \Delta\tau_C$ constant, the uncertainty is found to decrease with time in connection with the increase of $\tau_I - \tau_C$ the difference of time of flights (see figure 4). Considering a constant value of front velocity $v_i = 9.23$ mm.h^{-1}, the evolution in time of the uncertainty can be estimated by:

$$\frac{\Delta(c_s/c_l)}{c_s/c_l} = \frac{\Delta\tau}{2v_i(t-t_0)}(c_l + 2c_s) \tag{4}$$

This expression also gives a decrease with time and could in principle be reduced to very small values, while the ratio c_s/c_l is seen to converge to a value around 2.1 after 1 hour of solidification, as can be seen with the red shaded area in figure 5(b). A zoom between $t = 15$ and $t = 45$ min is shown in the inset of figure 5(b). The two solid black lines are the upper and lower values of the ratio c_s/c_l with $c_l = 3920$ m.s^{-1} and $c_s \in [7630, 8600]$ m.s^{-1}. We can clearly see that the observed dispersion is well estimated by this simple approach. Unfortunately, the error bars at the end of the run remain slightly larger than the difference between the values of c_s for (1 1 1) and (1 0 0) orientations. Indeed, the experimental data oscillate between these bounds with a mean value at $\langle c_s/c_l \rangle = 2.05 \pm 0.22$, which gives $\langle c_s \rangle = 8036$ m.s^{-1} $\pm$ 10%. This value is not close to any specific crystal orientation: the conclusion is that the grown ingot is most likely multi-crystalline, as expected for such a small amount of silicon. Note that this experiment was not initially designed to accurately measure the celerity in the solid. But it is clear from equation (4) that reducing the uncertainty on c_s significantly below the range $[c_s(1\ 1\ 1), c_s(1\ 0\ 0)]$ is possible, in particular in a bigger apparatus with a larger ingot thickness. Getting valuable inline information on the crystalline orientation is thus at reach.

5. Post-mortem crystal orientation analysis

As the silicon load is fully melted before starting the cooling ramp, there should not be a preferential grain orientation at nucleation, and due to the reduced size of the crucible, polycrystalline configuration is rather likely to occur. Nevertheless, as growth proceeds, grain selection may take place, with the (1 1 1) orientation expected to be dominant as stated in the reference [7]. On the other hand, with a relatively small ingot as ours, this grain selection mechanism can not be expected to be fully efficient and it can be expected that the grain structure should remain polycrystalline. To address the question of crystal orientation, EBSD (Electron Back Scattering Diffraction) has been conducted on the silicon ingot. A slice has been cut at height located at 3 mm and 7 mm, which roughly correspond to the middle and end of the front tracking experiment. Both faces of the slice obtained have been polished and prepared for the analysis. A centered disk of 10 mm diameter has then been scanned by juxtaposing passes of smaller dimensions to cover the whole area. This choice is justified by the fact that the carbon glass waveguide has a 10 mm diameter and, considering that diffraction of the ultrasound beam is small, the area sampled by the ultrasonic beam is a cylinder of 10 mm diameter. The results are shown in figure 6 in the form of EBSD-IPF (Inverse Pole Figure) maps for both faces of the slice. Colors are classically coded with respect to the main grain orientations.

Around 2300 grains have been detected on the lower face whereas 1300 grains have been counted on the upper face of the same area, showing an increasing grain size as

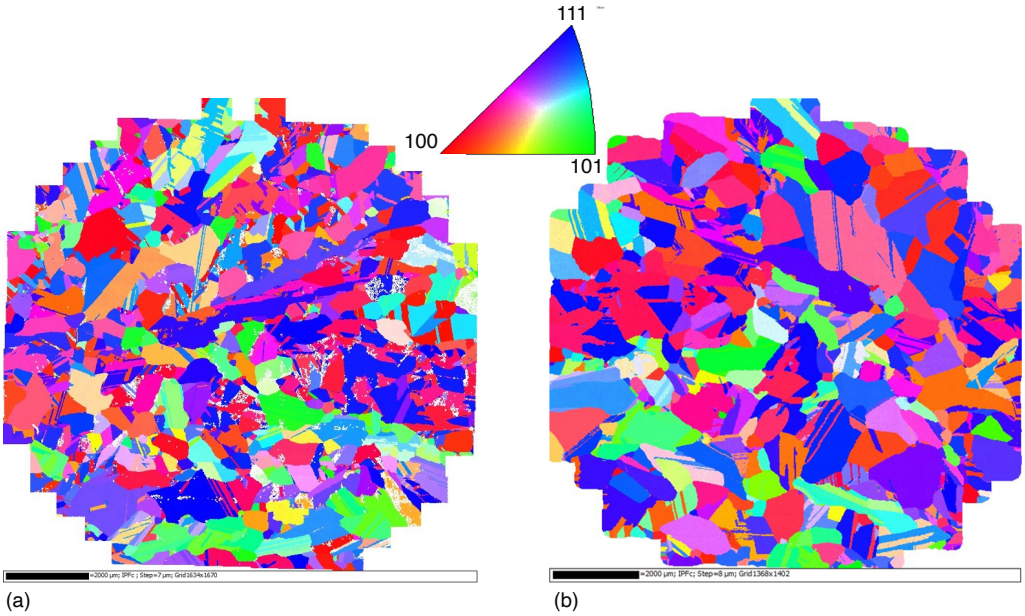

Figure 6: EBSD-IPF maps of 10 mm diameter area the solidified ingot (a) at 3 mm height ($t \sim 20$ min), 26% of the scanned area corresponds to grains close to the (1 1 1) orientation, 16% to grains close to the (1 0 0) orientation, no other orientations representing more than 10% of the investigated area. (b) at 7 mm height ($t \sim 46$ min), 30% of the scanned area corresponds to grains close to the (1 1 1) orientation, 17% to grains close to the (1 0 0) orientation, no other orientations representing more than 10% of the investigated area.

the crystal grows. A first observation is that the ingot is multi-crystalline without a dominant orientation of the grains. The (1 1 1) grain orientation, however, appears to have a slightly larger occurence than the other orientations for both faces. It becomes more dominant for the upper face as it could be expected for this low growth rate ([7]). The acoustic echoes travelling through the silicon solid phase are sensitive to the sound celerity of the material. To account for the dependency of the celerity on the grain orientation, we have associated a value of sound celerity to each fundamental color in the RGB system. And, as a first approximation, we have then considered that the celerity in a grain can be computed from its color coordinates in the RGB system. Repeating the procedure for each pixel of the image gives then a surface weighted average estimate of the celerity. The obtained estimate for both sides of the slice is comparable and equal to $c_s \simeq 8200$ m.s^{-1}. The relative difference with the experimental value obtained with times of flight analysis is only 2%.

6. Discussion and conclusion

The paper presents a technique to track the solid-liquid interface of photovoltaic silicon during directional solidification via ultrasound echo analysis. Acoustic bursts are introduced in the melted silicon thanks to a specifically-designed cylindrical waveguide. The material of the waveguide, carbon glass, ensures an excellent affinity and acoustic

matching with liquid silicon, and should result in acceptable contamination levels in the melt. An important advantage of this material relies on the reusability of the waveguide. It has been tested during several experimental runs (not all presented here), representing several cumulated hours of usage in melted silicon, without any damage.

The (s-l) interface is detected despite the low value of the reflection coefficient between liquid and solid silicon, thanks to a favorable signal to noise ratio. The signal from this interface is clear enough to make this technique potentially scalable to larger configurations. The echo analysis provides a very fast method to track the interface. The ease of implementation of this analysis, running on a laptop computer, opens the possibility to follow in line the position of the interface during solidification and to identify the velocity of the front. The accuracy of the ultrasound technique overrides manual or automated dipping techniques to track the interface position. The present experiment was dedicated to check the feasibility of emitting and receiving an echo from the (s-l) front with our decimetric, reusable waveguide. The goal has clearly been reached. Beyond the interface tracking, our technique provides an insight into the solidifying ingot by estimating the average sound wave celerity in the crystal, an information usually available only in *post-mortem* analysis. This is made possible by: i) a high transmission coefficient between liquid and solid silicon, ii) a high reflection coefficient on the crucible bottom (this depends on the crucible and furnace material and design) and iii) a relatively significant dependence of the sound celerity on crystal orientation. We showed that having an insight in average crystal orientation is within reach and that the accuracy of the result is dependent on the design of the furnace, the choice of the signal and the duration of the solidification. The reduction of the uncertainties is based on the increase of the acoustic frequency and of the duration of experiment. The first factor not only decreases $\Delta\tau$, the uncertainty on the time of flight but also reduces the interference effect when the solid thickness is close to the wavelength of the ultrasound. As the uncertainty on the times of flight detection decreases with time as $1/t$, the estimation of c_s gets better as the solidification advances, giving the possibility to eventually reach a value of c_s allowing to differentiate the average grain orientation of the grown crystal.

With the insurance of a good transmission of ultrasounds within liquid and solid silicon, further promising perspectives may be investigated such as the in-line detection of defaults.

Other perspectives of this work concern the optimization of the waveguide [35] in order to access to finer diagnostics as well as the possibility to perform *in situ* ultrasound doppler velocimetry [16, 36, 37, 38], giving velocity profiles of the flow in the melt. As mentioned in the introduction, a step forward in the use of ultrasounds in melts like Si is to act on the flow to enhance or control the concentration of impurities by acoustic streaming [23, 39, 40].

The ability of this prototype waveguide to produce acoustic streaming has been tested in water. Though the acoustic transmission coefficient is less favorable in water than for liquid silicon, this ability is illustrated in figure 7, which shows the jet flow (Eckart streaming) generated by the continuous emission of sinusoidal sound waves from the tip of the waveguide.

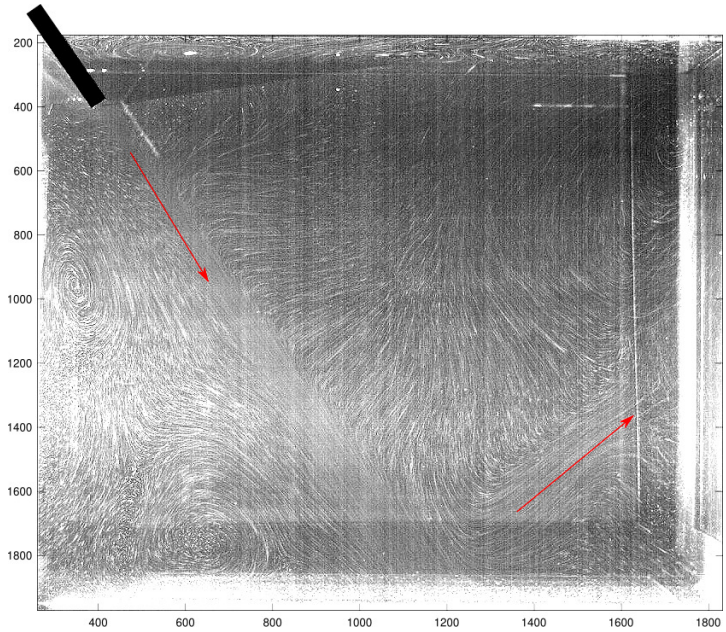

Figure 7: Average over 250 images of the flow generated by 4 MHz ultrasound wave coming out from the tip of the waveguide in a water tank.

7. Acknowledgements

This work was carried out as part of the ASTRES and BRASSOA projects supported by the institut Carnot Ingénierie@Lyon and AWINSI project by Ingénierie@Lyon and Énergies du Futur. The authors thanks Benoît Viniere for his preliminary work on data analysis, Beatrice Drevet for fruitful discussion, Damien Ponthenier for the induction furnace setup and Benoît Marie for conducting the EBSD analysis. The authors want to thank the anonymous referees for their suggestions improving the manuscript.

References

[1] K. Grujic, T. Hegna, K. Laundal, In situ monitoring of growth interfaces: A review of noninvasive methods, JOM 64 (2012) 96–101. doi:https://doi.org/10.1007/s11837-011-0233-9.

[2] D. Queheillalt, H. Wadley, Laser ultrasonic sensing of the melting and solidification of cadmium telluride, Journal of Crystal Growth 225 (2001) 34–448. doi:https://doi.org/10.1016/S0022-0248(01)01027-2.

[3] R. Morales, K. Harke, J. Tringe, D. S. T. Murray, Real-time laser ultrasonic monitoring of laser-induced thermal processes, Sci Rep 12 (2022) 9865. doi:https://doi.org/10.1038/s41598-022-13940-5.

[4] V. Bojarevics, G. Djambazov, K. Pericleous, Contactless ultrasound generation in a crucible, Metallurgical and Materials Transactions A 46 (2015) 2884–2892.
[5] K. Pericleous, V. Bojarevics, G. Djambazov, A. Dybalska, W. Griffiths, C. Tonry, Shape Casting, M. Tiryakioğlu, W. Griffiths and M. Jolly (eds.) Edition, Springer International Publishing, 2019.
[6] K. Fujiwara, K. Nakajima, T. Ujihara, N. Usami, G. Sazaki, H. Hasegawa, S. Mizoguchi, K. Nakajima, In situ observations of crystal growth behavior of silicon melt, Journal of crystal growth 243 (2002) 275–282.
[7] K. Fujiwara, Y. Obinata, T. Ujihara, N. Usami, G. Sazaki, K. Nakajima, In-situ observations of melt growth behavior of polycrystalline silicon, Journal of crystal growth 262 (2004) 124–129.
[8] K. Fujiwara, Y. Obinata, T. Ujihara, N. Usami, G. Sazaki, K. Nakajima, Grain growth behaviors of polycrystalline silicon during melt growth processes, Journal of crystal growth 266 (2004) 441–448.
[9] R. Parker, J. Manning, Application of pulse-echo ultrasonics to locate the solid/liquid interface during solidification and melting, Journal of Crystal Growth 79 (1986) 341–353. doi:https://doi.org/10.1016/0022-0248(86)90460-4.
[10] P. Dold, M. Heidler, A. Drevermann, G. Zimmermann, In situ observation of growth interfaces by ultrasound, Journal of Crystal Growth 256 (2003) 352–360. doi:https://doi.org/10.1016/S0022-0248(03)01405-2.
[11] A. Drevermann, C. Pickmann, R. Tiefers, G. Zimmermann, Online process control for directional solidification by ultrasonic pulse echo technique, Ultrasonics 42 (2004) 105–108. doi:https://doi.org/10.1016/j.ultras.2004.01.010.
[12] A. Drevermann, L. Sturz, N. Warnken, G. Zimmermann, Investigation of the initial transient in directional solidification of binary alcu alloys, Materials Science and Engineering: A 413–414 (2005) 259–262. doi:https://doi.org/10.1016/j.msea.2005.08.164.
[13] I. Ihara, D. Burhan, Y. Seda, Ultrasonic sensing of solid-liquid interface during directional solidification of aluminum, 1st International Conference on Sensing Technology (2005) 626–631.
[14] D. Burhan, I. Ihara, Y. Seda, In situ observations of solidification and melting of aluminum alloy using ultrasonic waveguide sensor, Mater. Trans. 46 (2005) 2107–2113. doi:https://doi.org/10.2320/matertrans.46.2107.
[15] I. Ihara, H. Aso, D. Burhan, In-situ observation of alumina particles in molten aluminum using a focused ultrasonic sensor, JSME International Journal Series A Solid Mechanics and Material Engineering 47 (2004) 280–286.
[16] S. Eckert, G. Gerbeth, V. Melnikov, Velocity measurements at high temperatures by ultrasound doppler velocimetry using an acoustic wave guide, Experiments in Fluids. 35 (2003) 381–388. doi:https://doi.org/10.1007/s00348-003-0606-0.
[17] S. Eckert, G. Gerbeth, Velocity measurements in liquid sodium by means of ultrasound doppler velocimetry, Experiments in Fluids. 32 (2002) 542–546. doi:https://doi.org/10.1007/s00348-001-0380-9.
[18] P. Jarry, M. Rappaz, Recent advances in the metallurgy of aluminium alloys. part i: Solidification and casting, Comptes Rendus Physique 19 (2018) 672–687. doi:https://doi.org/10.1016/j.crhy.2018.09.00.
[19] G. Lebon, G. Salloum-Abou-Jaoude, D. Eskin, I. Tzanakis, K. Pericleous, P. Jarry, Numerical modelling of acoustic streaming during the ultrasonic melt treatment of direct-chill (dc) casting, Ultrasonics Sonochemistrydoi:https://doi.org/10.1016/j.ultsonch.2019.02.002.
[20] D. Eskin, Ultrasonic melt processing: Achievements and challenges, MSF 828–829 (2015) 112–118. doi:https://doi.org/10.4028/www.scientific.net/MSF.828-829.112.
[21] M. Trempa, M. Hinderer, I. Kupka, C. Reimann, J. Friedrich, P. Czurratis, In-situ measurement of the solid-liquid-interface during the growth of silicon ingots by the ultrasonic sound method, 33rd European Photovoltaic Solar Energy Conference and Exhibition.
[22] J.-P. Garandet, V. Botton, D. Camel, B. Drevet, Ultrasonic waveguide device suitable for use in a directional solidification furnace for silicon, International Patent number WO2011064390 (A1) (2011).
[23] B. Moudjed, V. Botton, D. Henry, H. B. Hadid, J.-P. Garandet, Scaling and dimensional analysis of acoustic streaming jets, Phys. Fluids. 26 (2014) 093602. doi:https://doi.org/10.1063/1.4895518.
[24] M. Chatelain, S. Rhouzlane, V. Botton, M. Albaric, D. Henry, S. Millet, D. Pelletier, J. Garandet, Towards wall functions for the prediction of solute segregation in plane front directional solidification, Journal of Crystal Growth 475 (2017) 55–69. doi:https://doi.org/10.1016/j.jcrysgro.2017.05.019.
[25] M. Chatelain, V. Botton, M. Albaric, D. Pelletier, B. Cariteau, D. Abdo, M. Borrelli, Mechanical stirring influence on solute segregation during plane front directional solidification, International

Journal of Thermal Sciences 126 (2018) 252–262. doi:https://doi.org/10.1016/j.ijthermalsci.2017.12.024.

[26] M. Albaric, V. Brize, V. Botton, S. Miralles, Sonde acoustique destinee a etre utilisee dans un four de solidification du silicium et son procede de fabrication, Patent number FR3074908 (A1) (2019).

[27] R. Deike, K. Schwerdtfeger, Reactions between liquid silicon and different refractory materials, J. Electrochem. Soc 142 (1995) 609. doi:https://doi.org/10.1149/1.2044109.

[28] R. Voytovych, R. Israel, N. Calderon, F. Hodaj, N. Eustathopoulos, Reactivity between liquid si or si alloys and graphite, Journal of the European Ceramic Society 32 (2012) 3825–3835.

[29] M. Hayashi, H. Yamada, N. Nabeshima, K. Nagata, Temperature dependence of the velocity of sound in liquid metals of group xiv, International Journal of Thermophysics 28 (2007) 83–9. doi:https://doi.org/10.1007/s10765-007-0151-9.

[30] W. Rhim, S. Chung, A. Rulison, R. Spjut, Measurements of thermophysical properties of molten silicon by a high-temperature electrostatic levitator, International Journal of Thermophysics 18 (1997) 459–469. doi:https://doi.org/10.1007/BF02575175.

[31] W. Rhim, K. Ohsakat, Thermophysical properties measurement of molten silicon by high-temperature electrostatic levitator: density, volume expansion, specific heat capacity, emissivity, surface tension and viscosity, Journal of Crystal Growth 208 (2000) 313–321. doi:https://doi.org/10.1016/S0022-0248(99)00437-6.

[32] W. Rhim, K. Ohsakat, Density and thermal conductivity measurements for silicon melt by electromagnetic levitation under a static magnetic field, International Journal of Thermophysics 28 (2007) 44–59. doi:https://doi.org/10.1007/s10765-007-0160-8.

[33] N. Yoshimoto, M. Ikeda, M. Yoshizawa, S. Kimura, Sound velocity of molten silicon, Physica B: Condensed Matter 219–220 (1996) 623–625. doi:https://doi.org/10.1016/0921-4526(95)00832-2.

[34] Mersen TM, Properties of popular mersen grades (2022).
URL https://www.graphite-eng.com/uploads/downloads/properties_of_popuar_mersen_grades_2.pdf

[35] F. Foudzi, I. Ihara, Numerical study on optimum design of a clad waveguide for ultrasonic pulse-echo measurements with high signal-to-noise ratio, Mechanical Engineering Letters 2 (2016) 15–00727. doi:https://doi.org/10.1299/mel.15-00727.

[36] G. Losev, I. Kolesnichenko, The influence of the waveguide on the quality of measurements with ultrasonic doppler velocimetry, Flow Measurement and Instrumentation 75 (2020) 101786. doi:https://doi.org/10.1016/j.flowmeasinst.2020.101786.

[37] N. Thieme, P. Bonisch, D. Meier, R. Nauber, L. Buttner, K. Dadzis, O. Patzold, L. Sylla, J. Czarske, The influence of the waveguide on the quality of measurements with ultrasonic doppler velocimetry, IEEE Trans. Ultrason., Ferroelect., Freq. Contr. 64 (2017) 725–735. doi:https://doi.org/10.1109/TUFFC.2017.2654124.

[38] L. Gorbunov, A. Pedchenko, A. Feodorov, E. Tomzig, J. Virbulis, W. Ammon, Physical modelling of the melt flow during large-diameter silicon single crystal growth, Journal of Crystal Growth. 257 (2003) 7–18. doi:https://doi.org/10.1016/S0022-0248(03)01376-9.

[39] N. El Ghani, S. Miralles, V. Botton, D. Henry, H. Ben Hadid, B. Ter-Ovanessian, S. Marcelin, Acoustic streaming enhanced mass transfer at a wall, International Journal of Heat and Mass Transfer 172 (2021) 121090.

[40] B. Vincent, S. Miralles, D. Henry, V. Botton, A. Pothérat, Experimental study of a helical acoustic streaming flow, Physical Review Fluids, to be published.